Solar Energy 193 (2019) 494–501

Contents lists available at ScienceDirect

Solar Energy

journal homepage: www.elsevier.com/locate/solener

High-efficiency *n*-type silicon PERT bifacial solar cells with selective emitters and poly-Si based passivating contacts

Don Ding[a], Guilin Lu[a,b], Zhengping Li[a], Yueheng Zhang[a], Wenzhong Shen[a,c,*]

[a] Institute of Solar Energy, and Key Laboratory of Artificial Structures and Quantum Control (Ministry of Education), School of Physics and Astronomy, Shanghai Jiao Tong University, Shanghai 200240, PR China
[b] Lu'an Photovoltaics Technology Co., Ltd, Shanxi 046000, PR China
[c] Collaborative Innovation Center of Advanced Microstructures, Nanjing 210093, PR China

ARTICLE INFO

Keywords:
c-Si solar cells
n-PERT bifacial
Poly-Si based passivating contacts
Nano-layer SiO_x
Selective emitter

ABSTRACT

Bifacial crystalline silicon (c-Si) solar cells have currently attracted much attention due to the front high-efficiency and additional gain of power generation from the back side. Here, we have presented *n*-type passivated emitter and rear totally-diffused (*n*-PERT) bifacial c-Si solar cells featuring front selective emitter (SE) and polysilicon (poly-Si) based passivating contacts. The SE formation was scanned with laser doping based on front boron-diffusion p^+ emitter. The poly-Si based passivating contacts consisting of nano-layer SiO_x of ~1.5 nm thickness grown with cost-effective nitric acid oxidation and phosphorus-doped polysilicon exhibited excellent passivation for high open-circuit voltage. We have successfully achieved the large-area (156 × 156 mm^2) *n*-PERT bifacial solar cells yielding top efficiency of 21.15%, together with a promising short-circuit current density of 40.40 mA/cm^2. Theoretical calculation has further demonstrated that the optimal thickness of SiO_x nano-layer will increase from 1.5 nm to 1.8 nm if the density of interface defect state decreases by one magnitude from 1×10^{10} cm^{-2}/eV, and the cell efficiency can be improved up to 24.64% with open-circuit voltage over 0.720 V by optimizing the parameters of functional materials and interface layers. The present work has indicated that the commercialization of low-cost and high-efficiency *n*-PERT bifacial c-Si cells is possible due to the processes compatible with existing production lines.

1. Introduction

Crystalline silicon (c-Si) based photovoltaic industry plays a more significant role in renewable energy sources field year by year, where high performance *n*-type passivated emitter and rear totally-diffused (PERT) bifacial c-Si solar cells have been recently identified as a promising candidate. This is due to their ability to eliminate the light-induced degradation caused by boron-oxygen complexes (Glunz et al., 2001), which is a severe problem in *p*-type c-Si solar cell counterparts (Rudolph et al., 2016; Fichtner et al., 2018), and to exhibit a lower sensitivity to metal impurities contamination such as Fe, Cr, Co, W, Cu, Ni, *etc* (Scht et al., 2007). More important is that the bifacial device formed through a so-called "H-pattern" grid (namely a substitute for the conventional full area Al print of monofacial counterpart) has capacity of providing additional power generation gain of 10–30% from the rear side (Fertig et al., 2016). The bifacial solar cell structure, combined with the double glass module technology, is a perfect match with the current industrial process for a better long-term reliability at a low cost.

The *n*-PERT solar cell conception was first proposed by Zhao et al. (2002), at UNSW in Australia (cell size 4 cm^2). In recent years, many laboratories and research institutions have made satisfactory progress in the exploitation of *n*-PERT bifacial c-Si solar cells, e.g., co-diffusion or co-annealing to decrease the number of high temperature steps of standard process (Blevin et al., 2014; Lanterne et al., 2015), ion implantation or plasma immersion ion implantation of p^+ emitters (Lanterne et al., 2014; Kiefer et al., 2016; Lerat et al., 2016), selective oxidation etch-back to remove dead layer and reduce contact-resistance (Du et al., 2017; Buchholz et al., 2017), as well as chemical rounding technology and $SiO_2/Al_2O_3/SiN_x$ stacks to enhance antireflection and passivation performance (Song et al., 2018; Huang et al., 2018). We have recently presented simplified industrial processes to fabricate high performance *n*-PERT bifacial solar cells by using boron tribromide (BBr_3) diffusion emitter and phosphorus (P) ion-implanted back surface field (BSF) in conjunction with screen printed contacts (Lu et al., 2017).

* Corresponding author at: Institute of Solar Energy, and Key Laboratory of Artificial Structures and Quantum Control (Ministry of Education), School of Physics and Astronomy, Shanghai Jiao Tong University, Shanghai 200240, PR China.
E-mail address: wzshen@sjtu.edu.cn (W. Shen).

https://doi.org/10.1016/j.solener.2019.09.085
Received 9 July 2019; Received in revised form 22 September 2019; Accepted 26 September 2019

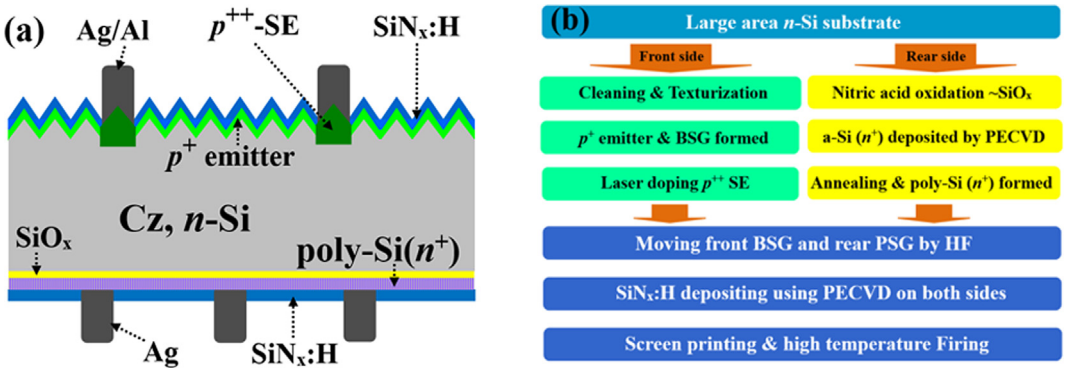

Fig. 1. (a) Schematic diagram and (b) main fabrication process of *n*-PERT bifacial c-Si solar cells with front p^{++} selective emitter and rear poly-Si based passivating contacts. The solar cells featuring a diffused B-doped emitter passivated by SiN_x:H antireflective coating using PECVD and by p^{++} selective emitter using laser doping on the front side, together with the ultra-thin SiO_x and n^+ poly-Si by nitric acid oxidation and PECVD on the back side, respectively. Note that the green area was designed for the front side, yellow area for the rear side, and blue area for both sides of the device in frabrication in both figures.

IMEC in Belgium has achieved the front average (44 cells) efficiency η of 22.4% with Ni/Ag co-plated contacts on both sides of large solar cells (size 239 cm^2) (Tous et al., 2017). The bifacial *n*-PERT solar cells are now mass-produced in Chinese photovoltaic companies of Yingli, Shanghai Shenzhou, Jolywood and Linyang with the front efficiency over 21% and bifaciality factor of 80–85% (size 6 in.).

However, the conventional *n*-PERT solar cells still face an improved bottleneck of cell efficiency which mainly lies in the carrier recombination loss at the metal/semiconductor Schottky contacts (Edler et al., 2015; Roemer et al., 2014; Cuevas et al., 2014). It is clearly desirable to expand the excellent passivation already demonstrated on c-Si surfaces to underneath the metal. Hydrogenated amorphous silicon (a-Si:H) or poly-Si based passivating contacts structure based on "selective blocking effect" (i.e., selectively block one carrier type while efficiently transporting the other carrier type) are both the effective ways to provide passivated contacts (Tanaka et al., 1992; Adachi et al., 2015; Yoshikawa et al., 2017; Feldmann et al., 2014a; Richter et al., 2015, 2017; Stodolny et al., 2016; Rienacker et al., 2017). Compared with a-Si:H heterojunction (deposition temperature is ~250 °C), the poly-Si based passivating contacts not only have recently attracted attention for their low recombination current densities (< 10 fA/cm^2) with maintaining sufficiently low contact resistivity, but also offer a considerably improved tolerance to high-temperature back-end metallization processes like screen printing and firing in *n*-PERT (Stodolny et al., 2016). Also, a-Si:H layer possesses relatively higher defect density which significantly reduces the cell short circuit current. The poly-Si based passivating contacts, e.g., tunnel oxide passivated contact (TOPCon), conception was first put forward by Feldmann et al. (2013), at Fraunhofer ISE in Germany. Recent progresses on poly-Si based passivating contacts include fabrication methods of ultra-thin silicon oxides (SiO_x) nano-layer, such as thermally or wet chemically grown interfacial oxide, ozone-based oxidation and field-induced anodization technologies (Feldmann et al., 2018a; Moldovan et al., 2015; Tong et al., 2015; Haase et al., 2018), carrier transport and recombination loss mechanism of interface passivating contacts between poly-Si and SiO_x (Feldmann et al., 2018a; Lozac'h et al., 2018; Feldmann et al., 2018b; Folchert et al., 2018), demonstration of better passivation effect of *n*-tunnel-oxide passivating contact than that of *p*-tunnel-oxide passivating contact (Feldmann et al., 2014b, 2014c), multicrystalline Si tunnel-oxide passivating contact solar cells (Schindler et al., 2015, 2017, 2018), as well as the combination of poly-Si based passivating contacts with interdigitated back contact structure (Peibst et al., 2014; Reichel et al., 2015; Young et al., 2016; Haase et al., 2018). Institute for Solar Energy Research has created the poly-Si based passivating contacts solar cells with champion efficiency reaching up to 26.1% by applying layer-selective laser process, as well as the cell efficiency of 25.7% for *n*-PERT solar cells in Fraunhofer ISE (both sizes 4 cm^2) (Richter et al., 2017; Haase et al., 2018).

The combination of *n*-PERT bifacial and poly-Si based passivating contacts must be an innovative and significative work for next generation c-Si based photovoltaic technology. Nevertheless, one of the main challenges of c-Si solar cells with this composite structure lies in the formation and integration of nano-scale SiO_x dielectric layer on routine large-area wafers. Existing studies have proved that if the quality of silicon oxide is not good, the electrical performance of the solar cells will be greatly reduced (Feldmann et al., 2018a, 2018b). In this work, we have demonstrated the prospective *n*-PERT bifacial c-Si solar cells featuring rear poly-Si based passivating contacts, together with front laser doping selective emitter (SE). The laser doping was performed to reduce carrier recombination on front borosilicate glass (BSG) surface based on conventional B-diffusion p^+ emitter for the sheet resistance of 110 Ω/□ (without low pressure diffusion equipment to form high sheet resistance, such as more than 130 Ω/□). Using the cost-effective nitric acid oxidation (while thermal oxidation requires specialized high-cost equipment), we have successfully grown nano-layer (~1.5 nm) SiO_x on large-area Si wafers with good uniformity and densification. After proper edge isolation and high temperature annealing, the properties of front and back configurations of the solar cells were able to be optimized simultaneously (without interfering with each other). The high performance large-area (156 × 156 mm^2) *n*-PERT bifacial c-Si solar cells with poly-Si based passivating contacts have been finally achieved in the process technologies compatible with current industrial production lines with the champion efficiency of 21.15%. Theoretical calculation with AFORS-HET (Automat FOR Simulation of HETerostructures) v2.5 agrees well with the experiment data, where an effectively way has been found to increase the cell efficiency of reaching up to 24.64%.

2. Experimental and simulation details

As starting materials, we employed commercial-grade *n*-type pseudo-square (156 × 156 mm^2) (1 0 0)-oriented Czochralski (Cz) c-Si wafers with an average thickness of 180 μm and resistivity of 0.5–3.0 Ω·cm. Fig. 1(a) and (b) shows the schematic structure and main production process, respectively, used in this study to demonstrate the applicability of laser doping SE and poly-Si based passivating contacts to high-efficiency *n*-PERT bifacial c-Si solar cells.

2.1. Fabrication of n-PERT bifacial solar cells with front SE structure (the rear side was replaced by BSF)

For *n*-PERT bifacial solar cells with only SE structure (cell schematic is omitted for clarity), firstly, the damage on both surfaces induced by wire-cutting was etched of ~10 μm per side in NaOH solution (10% by

volume) at 80 °C. After that, a wet-chemical process with alkaline solution was applied to create the random pyramids surface texture, followed by a standard wet-chemical cleaning sequence of RCA 1 and 2. All the samples needed to undergo BBr_3 diffusion back to back via a conventional high-temperature tube furnace (E2000 HT 300-5, Centrotherm, Germany), where only the outside of the wafers could be effectively diffused. The p^+ emitter with sheet resistance of ~110 Ω/□ and junction depth of ~0.7 μm was then formed.

The front surface was subsequently subjected to local heavy doping with nanosecond pulse laser for the wavelength of 532 nm and pulse energy in the range of 80–300 μJ (TPC/TSC series, Tsemc, China), resulting in rapid B-ions propulsion from the BSG layer into p^+ emitter and forming the p^{++} emitter. Note that the laser scanning lines location corresponded to the fine screen-printed grid lines. The line width of laser scanning (~160 μm) was required to exceed that of screen printing (~50 μm) for the purpose of reducing the difficulty of electrode alignment as well as improving the efficiency in printing. Afterward residue BSG layer was removed using diluted hydrofluoric acid solution (5% by volume), followed by the plasma edge isolation and rear polishing treatment with a mixture of hydrofluoric acid and nitric acid solution.

For the quasi-planar back side, P ions were implanted with an acceleration voltage of 15 keV and a dose of 3.2×10^{15} cm^{-2} (IonSolar™, Kingstonesemi, China). And then, conventional oxidation process (800 °C, 30 min) was employed to activate dopants for the formation of n^+ BSF with the junction depth of 0.85 μm, sheet resistance of 37 Ω/□ and surface concentration of ~2.19×10^{20} cm^{-3}. Hydrogenated silicon nitride SiN_x:H (fixed thickness of 75 nm) antireflective coatings were deposited on both sides by PECVD (SINA XS, Roth & Rau, Germany). Finally, the front Ag/Al and rear Ag electrode grids were guaranteed by screen-printed metallization (LTCC, Baccini, Italy), together with a co-firing in an infrared belt-furnace (CFD-9024, Dispatch, USA).

2.2. Fabrication of n-PERT bifacial solar cells with rear poly-Si based passivating contacts (no SE structure in the front side)

The *n*-PERT bifacial c-Si solar cells with only poly-Si based passivating contacts were fabricated from the same Si materials (cell schematic is omitted for clarity). For the front side, conventional BBr_3 diffusion with high-temperature tube furnace was employed to prepare p^+ emitter after damage etching, alkaline texturing and RCA clean. The specific operation process was consistent with the previous part, but laser doping SE was not introduced here. For the polished back side, ultra-thin SiO_x layer was grown in boiled 68 wt% nitric acid at 80 °C for 20 min, then covered by poly-Si layer crystallized from 90 nm thick P-doped a-Si:H layer using a parallel-plate PECVD with deposition temperature of 250 °C (Pine-m-R-5, Ideal Energy, China) and annealing treatment. Note that the final thickness of n^+ ploy-Si was thinner than 90 nm after moving phosphorosilicate glass (PSG). The number of wafers in each tray was fixed at 50. Subsequent steps such as the deposition of SiN_x:H (fixed thickness of 75 nm) antireflective coatings on both sides, front Ag/Al and rear Ag contact electrodes were also done to form a complete bifacial c-Si solar cell.

2.3. Fabrication of n-PERT bifacial solar cells with both SE and poly-Si based passivating contacts

The complete *n*-PERT bifacial c-Si solar cells with both SE and poly-Si based passivating contacts were also manufactured to minimize the carrier recombination loss and improve the interface passivation (see Fig. 1(a) and (b)). Briefly, the front surface was first doped with boron through high-temperature tube furnace to form p^+ emitter, and laser doping was subsequently employed to generate p^{++} SE through pushing B-ions from BSG into Si layer. Then nitric acid oxidation and PECVD were used to produce ultra-thin SiO_x layer and as-deposited a-Si:H layer at the back side. A high-temperature P-diffusion and annealing treatment should be adopted to facilitate the crystallization from a-Si:H into n^+ poly-Si. Finally, we deposited SiN_x:H antireflective coatings on both surfaces, Ag/Al and Ag contact electrodes on front and back surfaces, respectively. The detailed production process of each step had been mentioned above.

2.4. Characterization

The thickness and refractive index of SiN_x:H and SiO_x layers were extracted from spectroscopic ellipsometry (400 adv-PV, Sentech, Germany). The doping profiles in p^{++} SE and n^+ poly-Si based passivating contacts were measured by electrochemical capacitance-voltage (ECV) profiling (CVP21, WEP, Germany), and the sheet resistance were determined by 4-point probes (280I Series, Four Dimensions Inc., USA). The external quantum efficiency (*EQE*) was received on the platform of quantum efficiency measurement (QEX10, PV Measurements, USA). The implied open-circuit voltage (implied-V_{OC}) and effective minority carrier lifetime (τ_{eff}) of the cell precursors were obtained by quasi-steady-state photo-conductance (QSSPC) method (WCT-120, Sinton Instruments, USA) in the transient or generalized mode. The electrical properties (V_{OC}, short-circuit current J_{SC}, fill factor *FF*, and energy conversion efficiency η) of *n*-PERT bifacial c-Si solar cells were measured under standard test condition with a steady-state solar cell *I-V* tester (Industrial Vision Technology, VS-6820) equipped with a class AAA solar simulator.

2.5. Simulation parameters setting

AFORS-HET v2.5 developed by Helmholtz-Zentrum Berlin is a very powerful and professional numerical simulation tool for the heterojunction c-Si solar cells (e.g., poly-Si based passivating contacts solar cell is also a heterojunction). On the one hand, carrier transport route of solar cell with poly-Si based passivating contacts has one-dimensional characteristic which is perfectly matched with AFORS-HET software. On the other hand, carrier transportation through SiO_x dielectric layer can be described herein by two mechanisms: the thermionic-emission and thermionic field model, as well as the hetero-interface quantum tunneling model. The SiN_x:H/c-Si(p^+) and SiN_x:H/poly-Si(n^+) stacks were modelled as MS-Schottky contacts, together with flat band of metal work function being set in the front contact boundary. We emphasized further that the input parameters of the optical and electrical layers were from the experimental data or default value in the software, including the available c-Si wafer thickness of ~160 nm, *n*-type bulk resistivity of ~1.5 Ω·cm, p^+ emitter with the peak substitutional dopant concentration of 2×10^{19} cm^{-3} and junction depth of ~0.7 μm, as well as refractive index (*n*) and extinction coefficient (*k*) of c-Si and SiN_x:H materials. The generation of electron/hole pairs can be described by taking Lambert-Beer absorption into account. Note that the bandgap narrowing effect had already been considered in this calculation mode. The specific solar cell parameters used in AFORS-HET simulation are shown in Table 1, where *d* is the thickness, *SRV* the surface recombination velocity, N_{p+} the acceptor concentration, N_n and N_{n+} both the donor concentration, N_{tr} the density of bulk defect state, D_{it} the density of interface defect state, *Chi* the electron affinity energy, E_g the band gap, d_k the relative dielectric constant, m_e and m_h the effective mass factor for tunneling of electron and hole, respectively, D_{ph} the pinhole density through the insulator layer (dimensionless unit), and w/o means without.

3. Results and discussion

3.1. Influence of front laser doping SE on cell performance

As we know is that carrier recombination in doped regions of a solar cell places a major limit on its performance. The front emitters doped heavily under metal contacts can offer a route toward lower recombination and higher efficiency via low resistivity Ohmic contact

Table 1
Input parameters of *n*-PERT bifacial c-Si solar cells with TOPCon stacks used for the simulation of optimized results.

Layers	Default parameters
SiN_x dielectric	d = 75 nm (front and back side)
Front contact boundary	Standard Si ⟨1 1 1⟩ pyramids (54.74°), w/o absorption loss, fix metal work function to flat band
Flat band Schottky front interface	MS-Schottky contact, front SRV = 10 cm/s (fitted value from experiment, including laser doping p^{++} SE)
c-Si(p^+) layer	d = 0.7 μm, N_{p+} = 2 × 10^{19} cm^{-3}, N_{tr} = 1 × 10^{10} cm^{-3}/eV
n-type c-Si layer	d = 160 μm, N_n = 3.2 × 10^{15} cm^{-3}, ρ = 1.5 Ω cm, N_{tr} = 8 × 10^9 cm^{-3}/eV
Insulator SiO_x (interface)	Thermionic emission and thermionic field mode, d = 1.5 nm, Chi = 1.0 eV, E_g = 8.9 eV, D_{ph} = 1 × 10^{-8}, d_k = 3.9, m_e = 0.98, m_h = 0.49, D_{it} = 1 × 10^{10} cm^{-2}/eV
poly-Si(n^+) layer	d = 90 nm, N_{n+} = 3 × 10^{18} cm^{-3}, N_{tr} = 2 × 10^{11} cm^{-3}/eV
Flat band Schottky back interface	MS-Schottky contact, rear SRV = 1 × 10^5 cm/s
Back contact boundary	Plane surface, w/o absorption loss, fix metal work function to flat band

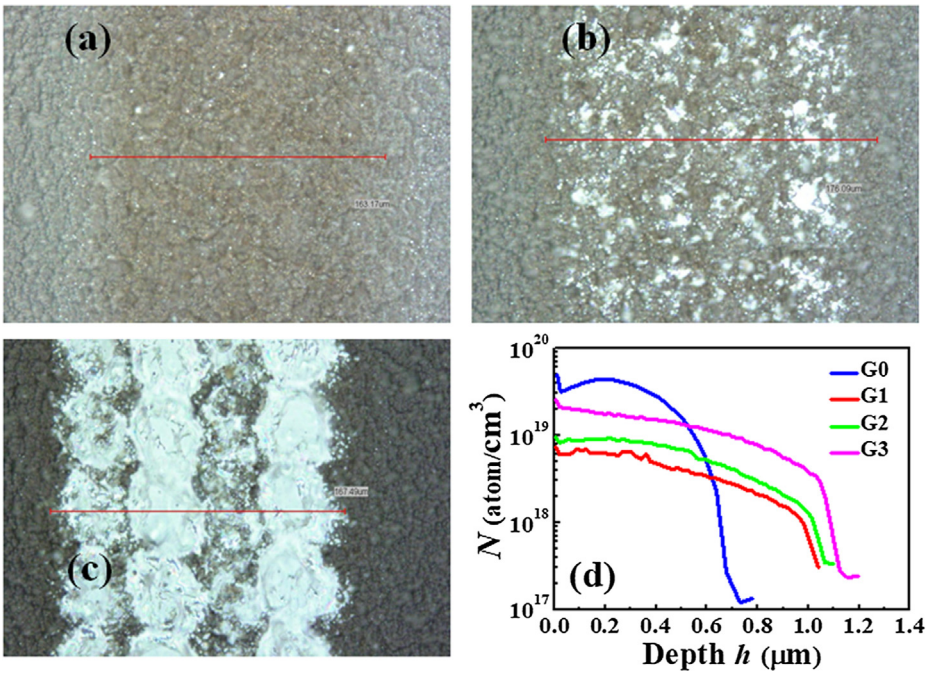

Fig. 2. (a-c) Front surface morphology of silicon wafers and (d) ECV doping profiles of the front p^{++} selective emitter after different laser energy scanning without annealing treatment. The ever-increasing laser energy of 80–300 μJ for groups G1-G3 acts on the front surface against the reference group G0 without laser doping.

(i.e., band-bending effect), which is different from the emitter doped relatively lower between metal contacts reducing losses from Auger recombination. Fig. 2(a-c) exhibited the front surface morphology of silicon wafers swept by three kinds of laser with different energies of groups G1-G3. The thin line width of swept area was about 170 μm. The surface doping concentration and doped junction type were measured by CVP21 after the surface BSG was removed with diluted HF solution. Fig. 2(d) presented the wafer ECV dopant profiles of the laser doping SE versus various laser energy groups of G0, G1, G2 and G3 without annealing treatment. The laser energy of groups G1-G3 gradually increased in the range of 80–130 μJ, while group G0 corresponded to the reference group without laser doping. The SE regions of groups G1 and G3 exhibited the surface concentration of ~0.85 × 10^{19} cm^{-3} and ~2.90 × 10^{19} cm^{-3} with the junction depth h of ~1.08 μm and ~1.22 μm, respectively, while group G0 showed a great distinction for the surface concentration of ~0.51 × 10^{20} cm^{-3} and the h of ~0.77 μm. Obviously, the higher the laser energy, the deeper the *p-n* junction was pushed. Moreover, all the surface concentrations with laser doping were lower than that without laser doping. The reason is that plenty of B-ions were pushed deeper from the surface of localized melting Si substrate under laser irradiation (Jaeger et al., 2011).

We have evaluated the influence of laser treatment on the performance of *n*-PERT bifacial c-Si solar cells. Fig. 3(a-d) illustrated the electrical parameters (V_{OC}, J_{SC}, *FF*, and η) of solar cells with only front SE (no poly-Si based passivating contacts in the back side) versus groups G0-G3. The single-sided testing method was adopted to measure the front electrical performance of solar cells (i.e., contacting the front main grids of solar cells with metal probes, while the back side was contacted using light-proof metal table), therefore the effect of back lighting on the whole cells was excluded. Fig. 3(a) showed that the average V_{OC} of group G2 for ~0.645 V was higher than that of groups G1 and G3, demonstrating a best selection for right power laser. The group G2 had the optimal average J_{SC} of 39.2 mA/cm^2 seen in Fig. 3(b). For the lower laser energy, the built-in voltage is relatively weak compared with group G2 due to shallower laser-doped emitter, while the higher laser energy density disturbs silicon surface because of the ablation of silicon and increases the surface recombination after laser scanning. Moreover, thermal damage will be introduced into space charge region for higher laser, leading to the enhancement of recombination current in the space charge region (Hopman et al., 2009; Li et al., 2013). Improper laser doping would also increase the contact resistance of Ag/Al paste/p^+ emitter stack by changing the surface doping concentration, resulting in a lower *FF* value shown in Fig. 3(c). Fig. 3(d) finally illustrated that group G2 created the best solar cells with the average η of 20.15% and the top η of 20.3%.

In order to analyze the effect of different laser doping irradiations on properties of emitter area, we have further presented in Fig. 3(e) the *EQE* and reflectance (*R*) in conventional *n*-PERT bifacial solar cells

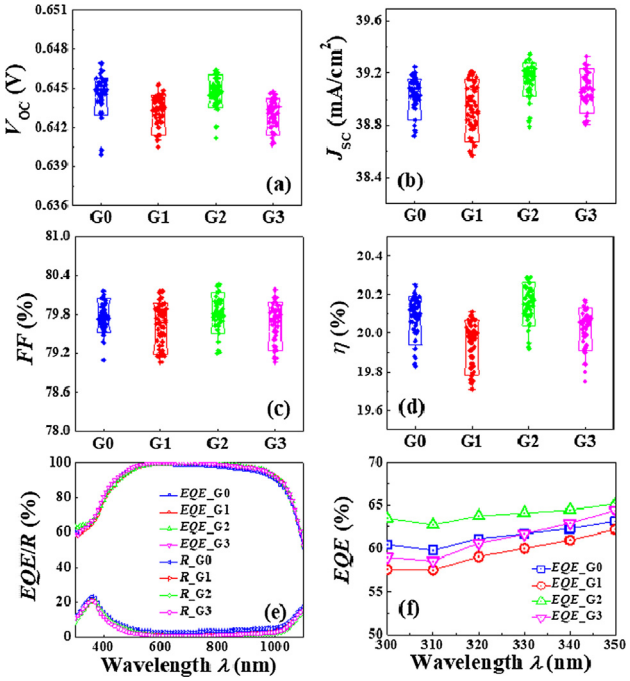

Fig. 3. (a-d) Box plot of electrical parameters (V_{OC}, J_{SC}, *FF* and η) for the bifacial c-Si solar cells after laser scanning. (e) Measured *EQE* and *R* of bifacial c-Si solar cells against the wavelength of 300–1100 nm. (f) Measured *EQE* enlarges the difference in the short wavelength of 300–350 nm. Note that the back side of the solar cells was set to conventional n^+ BSF structure without poly-Si based passivating contacts. The line width of laser scanning is 160 μm, while 50 μm width for metallization grids.

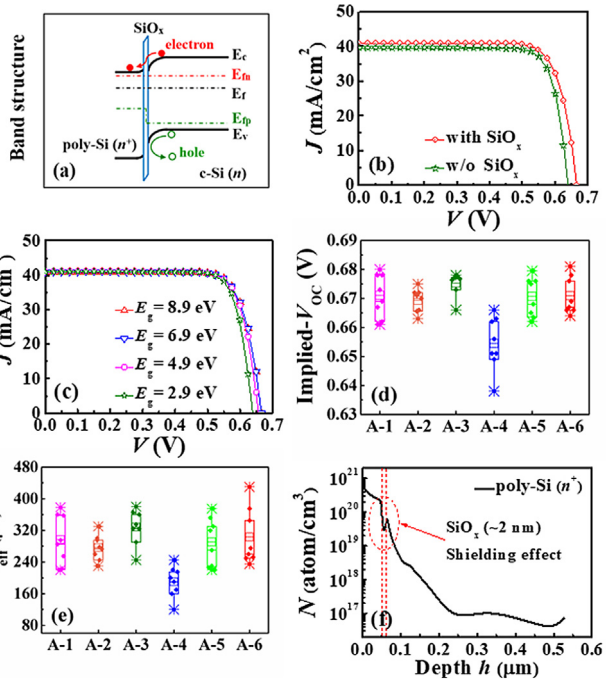

Fig. 4. (a) Band diagram of the poly-Si(n^+)/SiO_x/c-Si(n) stacks in thermal equilibrium. Modeled current–voltage (*J-V*) curves for *n*-PERT bifacial c-Si solar cells (b) with or without rear SiO_x insulating layer and (c) versus various energy gap E_g values (2.9, 4.9, 6.9 and 8.9 eV) caused by oxygen content. (d) Implied-V_{OC} and (e) effective carrier lifetime τ_{eff} of the solar cell's precursor with different annealing temperatures and annealing times (A-1: 890 °C/20 min, A-2: 910 °C/20 min, A-3: 930 °C/20 min, A-4: 890 °C/30 min, A-5: 910 °C/30 min, A-6: 930 °C/30 min). Note that the intrinsic carrier concentration n_i selected in the test was 8.6×10^9 cm^{-3} and injection concentration Δn was 3.0×10^{15} cm^{-3}. (f) Tested doping profile of phosphorus in the back-sided poly-Si(n^+)/SiO_x/c-Si (n) stacks to evaluate the performance of SiO_x.

(with the back side set to n^+ BSF structure without poly-Si based passivating contacts) versus these laser energies for the wavelength of 300–1100 nm. It can be seen that only group G2 contributed the *EQE* of exceeding 60% in the short wavelength of 300–350 nm (see Fig. 3(f)), indicating that the realization of higher utilization rate of front emitter on photons of sunlight with G2 treatment (group G2 produced the surface concentration of ~1.02×10^{19} cm^{-3} and the *h* of ~1.12 μm as shown in Fig. 2(d)). The influence of laser scanning on solar cell is not only reflected in dopant profiles, but also in front emitter and its passivation. Another important function of laser doping is to reduce the Auger recombination due to lower level emitter sheet resistance after laser scanning in light trapping spectral region. The same conclusion was drawn from the η observation in Fig. 3(d). In addition, groups G1-G3 exhibited the better *EQE* compared to group G0 in the middle-long wavelength of 600–1000 nm. This may be due to the fact that the micrometer-level pyramids can be converted to nanometer-level after laser scanning, leading to a lower reflectivity and therefore higher photon absorption.

3.2. Influence of rear poly-Si based passivating contacts on cell performance

Fig. 4(a) sketched the band diagram of poly-Si(n^+)/SiO_x/c-Si(n) structure in thermal equilibrium. The P-doped poly-Si layer was separated from c-Si substrate by an SiO_x nano-layer which has the capacity of reducing interface carrier recombination and preventing epitaxial regrowth of the as-deposited a-Si:H layer during high-temperature anneal. We have theoretically analyzed *n*-PERT bifacial c-Si solar cells with or without SiO_x (band gap E_g of 8.9 eV) to assess the importance of this ultra-thin insulating layer, as shown in Fig. 4(b). The density of interface defect state D_{it} for solar cells with tunnel oxide layer was set for 1×10^{10} cm^{-2}/eV (see in Table 1), while D_{it} of 3×10^{11} cm^{-2}/eV for solar cells without tunnel oxide layer. The current-voltage (*J-V*) curves exhibited that both J_{SC} and V_{OC} of solar cell with SiO_x were higher than those of solar cell without SiO_x (the J_{SC} was 1.34 mA/cm^2 higher, and V_{OC} 28 mV higher), supporting excellent carrier tunneling function and rear passivation quality. Existing results also suggested that this heterojunction structure with carrier selectivity can not only improve the blue response compared to a-Si/c-Si heterojunction, but also avoid the negative effects of high doping which are the causes of the intrinsically higher losses for conventional homojunction technology (Ghannam et al., 2013). The band gap E_g of SiO_x varies with the degree of oxidation. Fig. 4(c) presented the comparison of *J-V* curves for SiO_x materials with different E_g values. It can be seen that the tendency to reduce V_{OC} was getting faster as E_g decreased, while J_{SC} remained constant. We have therefore drawn the conclusion that the difference of oxygen content in SiO_x affects the interface passivation.

A high-temperature treatment should be adopted to facilitate the crystallization of as-deposited a-Si:H layer and to reduce the contact resistance between the metal electrode and doped Si. The annealing needed to be controlled to maintain the oxide's integrity and abrupt junction (i.e., dopant diffusion from poly-Si into c-Si layer should be prevented or limited to a tolerable level), as well as the activation of P-ions. In the experiment, we employed six annealing temperature/time sets: 890 °C/20 min (A-1), 910 °C /20 min (A-2), 930 °C/20 min (A-3), 890 °C/30 min (A-4), 910 °C/30 min (A-5) and 930 °C/30 min (A-6). Fig. 4(d) and (e) illustrated the corresponding implied open-circuit voltage (implied-V_{OC} and τ_{eff}) of the solar cell's precursor (non-metallization for the solar cell structure with conventional p^+ emitter without laser doping selective emitter). We can observe that increasing the annealing temperature from 890 °C to 930 °C would improve the implied-V_{OC} at first for fixed annealing time of 30 min, and then the increasing trend becomes slower (a similar variation was also observed

in τ_{eff}), which was in keeping with the *J-V* curves for various E_g values in Fig. 4(c). At the same time, the effect of annealing temperature was found to be greater than that of annealing time. We finally achieved the average implied-V_{OC} of over 0.670 V and average τ_{eff} of over 275 μs except group A-4.

As we know, when nitric acid or ozone-based oxidation is carried out on the back surface of Si substrate, oxygen atoms can fully contact with Si in reaction within the ultra-thin region away from the surface. The resulting tunneling oxide layer is supported to have a higher density due to more saturated Si-O bonds (2.11 g/cm^3 for nitric acid and 2.21–2.25 g/cm^3 for ozone-based oxides) and has the composition close to that of stoichiometric SiO_2 (Moldovan et al., 2015; Sugita et al., 1996; Moldovan et al., 2014). We implemented the Si wafers herein covered by nano-layer SiO_x with high E_g using nitric acid oxidation processing. Fig. 4(f) presented the ECV P-doped profiles in poly-Si(n^+)/SiO_x/c-Si(n) stacks after the annealing treatment of 910 °C/30 min. Apparently, the surface concentration of P-ions on the back side was 5.35 × 10^{20}/cm^{-3} decreasing slowly as the doping depth h increases, but sharply drop off in the depth range of 0.050–0.052 μm. This confirmed that the presence of insulating SiO_x layer for the thickness of ~2 nm prevented the diffusion of P-ions from poly-Si into c-Si layer (i.e., shielding effect). The thickness of SiO_x layer was determined by spectroscopic ellipsometry to be 1.5 nm thin. The concentration added from 2.48 × 10^{19} cm^{-3} to 6.15 × 10^{19} cm^{-3} with the h changed between 0.0524 and 0.0623 μm, illustrating some P-ions still passed through the insulating layer. The change of doping concentration distribution proved that this oxide layer has superior compactness and could be used for poly-Si based passivating contacts.

3.3. Comprehensive impact of the SE and poly-Si based passivating contacts

The electrical parameters (V_{OC}, J_{SC}, *FF*, η) of large-area (156 × 156 mm^2) *n*-PERT bifacial c-Si solar cells featuring front laser doping SE and rear poly-Si based passivating contacts have been taken into consideration in Fig. 5(a-d). It can be seen from Fig. 5(a) that group A-5 in 910 °C had the highest average V_{OC} of ~0.660 V, while the decreased V_{OC} would be occurred for group A-6 in 930 °C. This can be mainly explained with the local disruption of tunneling SiO_x nano-layer (SiO_2 accounts for the vast majority) in an oxygen-free ambient of higher temperature based on the reaction of SiO_2(s) + Si(s) → 2SiO(g), where the s and g denote solid and gaseous phase, respectively. The carrier-selective contact with a completely c-Si phase could not be

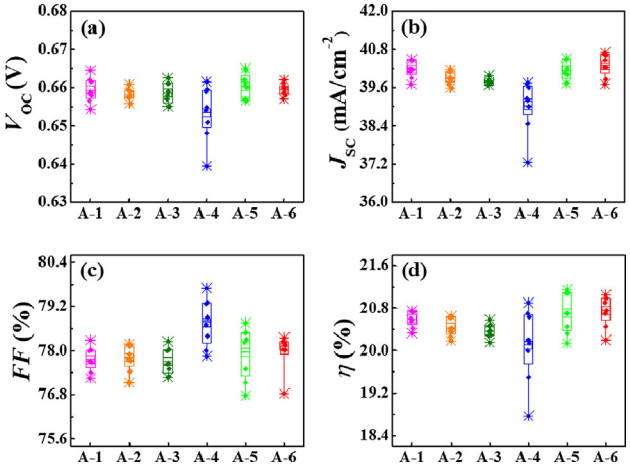

Fig. 5. Electrical parameters of (a) V_{OC}, (b) J_{SC}, (c) *FF* and (d) η for the different annealing temperatures and annealing times of groups from A-1 to A-6 (A-1: 890 °C/20 min, A-2: 910 °C/20 min, A-3: 930 °C/20 min, A-4: 890 °C/30 min, A-5: 910 °C/30 min, A-6: 930 °C/30 min). The device structure was a complete large-area (156 × 156 mm^2) *n*-PERT bifacial c-Si solar cell featuring front SE (laser energy of about 200 μJ) and back poly-Si based passivating contacts.

obtained (weaken the interface passivation) due to the balling-up of oxide (break the integrity of oxide) (Feldmann et al., 2014a,c). Moreover, comparing Fig. 5(a) with Fig. 3(a), the top V_{OC} of bifacial c-Si solar cells with poly-Si based passivating contacts (V_{OC} ~0.665 V) was 19 mV higher than that of solar cells without poly-Si based passivating contacts (V_{OC} ~0.646 V), resulting in an increase in top efficiency of 0.9% (absolute value). This demonstrated that poly-Si based passivating contacts played a significant role in interface passivation and carrier transport.

Fig. 5(b) presented that the J_{SC} of group A-5 was higher than that of group A-2, while group A-4 exhibited reverse trend compared to group A-1. This indicated that the higher temperature groups required longer annealing times for better passivation quality than the low temperature group. The *FF* in Fig. 5(c) showed the contrary trend compared to J_{SC}. The reason for *FF* limitation could be mainly ascribed to the following points: carrier recombination in the space charge region and at the SiO_x rear passivation layer for the large asymmetry in capture cross-sections (the cross sections of electrons captured by recombination centers are much larger than that of holes, namely $\sigma_n \gg \sigma_p$) affected by annealing temperature (Feldmann et al., 2014b), and presence of pinholes in the oxide. Therefore, the optimal annealing temperature had a compromised selection. The eventual outcome verified that the average V_{OC} of large-area *n*-PERT bifacial c-Si solar cells in groups of A-5 and A-6 was ~0.660 V, and the average η of ~20.7% (Fig. 5(d)), where the best electrical properties (V_{OC} ~0.665 V, J_{SC} ~40.40 mA/cm^2, *FF* ~78.75% and η~21.15%) was achieved in group A-5.

3.4. Theoretical analysis for tunneling characteristics of SiO_x layer

It is one of the challenges to prepare high-quality nano-layer SiO_x on a large-area Si substrate. We therefore needed to conduct an in-depth analysis to the impact of SiO_x on the performance of solar cells featuring front B-diffused emitter with theoretical simulation to find out the optimal SiO_x structure. Noted that AFORS-HET is the one-dimensional heterojunction simulation software, which cannot set up the two-dimensional structure like laser doping SE. An approximate treatment was adopted for SE, i.e., the simulated emitter junction parameters would be set to keep consistent with those of experimental solar cells by optimizing the surface recombination rate and B-doped sheet resistance. In fact, the object of study herein is poly-Si based passivating contacts, it is reasonable to keep a fixed value for front p^+ emitter. P-diffusion from the poly-Si layer into the c-Si substrate has not been taken into account in the simulations. Fig. 6(a-d) presented the overall electrical properties of the solar cells with various tunneling oxide thicknesses d and densities of state D_{it} at the interface between SiO_x and poly-Si layers. The default parameters of the solar cells were listed in Table 1. From Fig. 6(a), the V_{OC} was found to be sensitive to D_{it} and approached its upper-limited value and then basically stayed stable by increasing d, for which the reason could be attributed to the suppression of leak current by oxide at a higher thickness. Fig. 6(b) displayed that the J_{SC} would decrease rapidly as d exceeded its threshold value, proving the tunneling characteristics of carrier transport. The J_{SC} showed a rapid decline as d increased to 1 nm for the D_{it} of 1 × 10^{12} cm^{-2}/eV, while still maintained stable for the d reaching 2 nm with a lower D_{it} of 1 × 10^9 cm^{-2}/eV. Comparing with J_{SC}, *FF* was less susceptible to d and D_{it}, i.e., *FF* started to decay only at a larger d and lower D_{it} (see Fig. 6(c)). The trends of *Eff* in Fig. 6(d) were similar to those of J_{SC}, demonstrating that the size of the tunneling current had a momentous impact on cell efficiency. At d = 1.5 nm and D_{it} = 1 × 10^{10} cm^{-2}/eV, the calculative efficiency is 21.17% (illustrated in Fig. 6(d) with V_{OC} = 0.664 V, J_{SC} = 40.42 mA/cm^2 and *FF* = 78.85%), close to the best experimental result of 21.15% in group A-5 (see Fig. 5(d) with V_{OC} = 0.665 V, J_{SC} = 40.40 mA/cm^2 and *FF* = 78.75%). We can further expect that the optimal thickness of SiO_x layer will increase from 1.5 nm to 1.8 nm if D_{it} decreases by one magnitude from 1 × 10^{10} cm^{-2}/eV, which is benefit to the process technology of poly-Si based

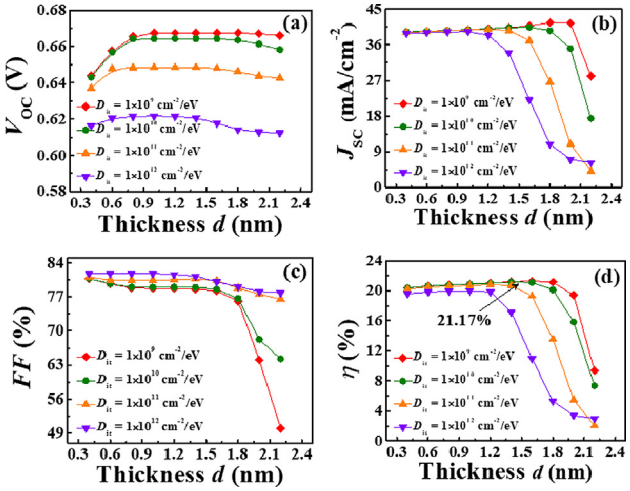

Fig. 6. Calculated electrical parameters of (a) V_{OC}, (b) J_{SC}, (c) *FF* and (d) η for different densities of interface state D_{it} (1×10^9, 1×10^{10}, 1×10^{11}, and 1×10^{12} cm^{-2}/eV) as a function of tunneling SiO_x thickness *d* ranging from 0.4 to 2.2 nm. The fixed parameters of simulated front emitter junction would be set to keep consistent with those of the experimental solar cells by means of optimizing the front surface recombination rate and sheet resistance of p^+ emitter.

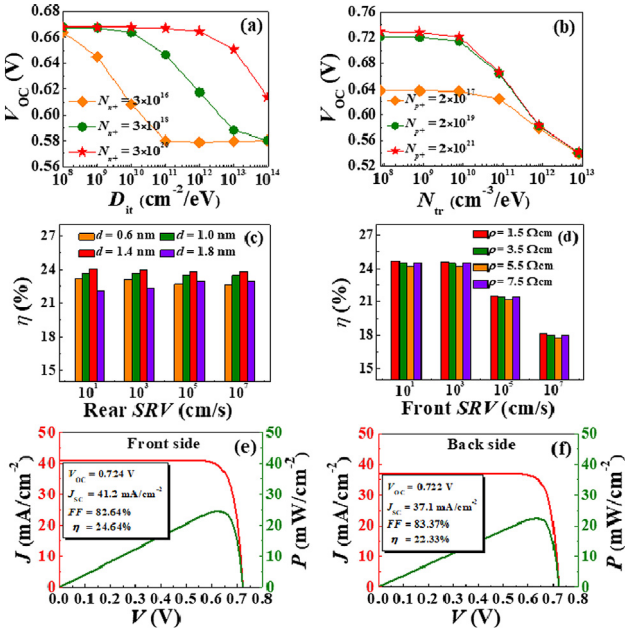

Fig. 7. Effect of (a) different densities of interface state D_{it} and (b) densities of bulk defect state N_{tr} of Si substrate on V_{OC} of the *n*-PERT bifacial c-Si solar cells with various doping concentrations of rear n^+ poly-Si (3×10^{16}, 3×10^{18} and 3×10^{20} cm^{-3}) and front p^+ (including p^{++} laser SE) emitter (2×10^{17}, 2×10^{19} and 2×10^{21} cm^{-3}). Enhancing effect of η versus various (c) rear surface recombination rate *SRV* and (d) front *SRV* with different SiO_x thicknesses *d* (0.6, 1.0, 1.4 and 1.8 nm) and Si substrate resistivities ρ (1.5, 3.5, 5.5 and 7.5 Ω·cm). Top efficiency of (e) front side η = 24.64% and (f) back side η = 22.33% of the investigated bifacial solar cells was finally obtained based on the parameters previously optimized.

passivating contacts solar cells.

3.5. Optimization

We have successfully achieved the large-area (156×156 mm^2) *n*-PERT bifacial c-Si solar cells with poly-Si based passivating contacts with over 21% efficiency and the best V_{OC} of 0.665 V. However, it is necessary and possible to find an effectively way to realize higher cell efficiency with superior V_{OC}, since the V_{OC} values of good poly-Si based passivating contacts solar cells have been reported exceeding 700 mV (Richter et al., 2017, 2018; Feldmann et al., 2014b). Some prerequisites need to be taken into consideration to yield the highly efficient passivated contacts for solar cells, i.e., excellent interface passivation and efficiently doped layers to maintain the quasi-Fermi level separation in c-Si for high V_{OC}, and an efficient majority carrier transport for high J_{SC} and *FF*. We have analyzed in Fig. 7(a) the effect of poly-Si doping concentrations N_{n+} and densities of state D_{it} at poly-Si/SiO_x interface on V_{OC}. It can be seen that the V_{OC} was enhanced with increasing N_{n+} or decreasing D_{it}, but no longer changed when it increased to a certain extent. For example, the V_{OC} was ~0.580 V for N_{n+} of 3×10^{18} cm^{-3} and D_{it} of 1×10^{14} cm^{-2}/eV, and then became stable after reaching ~0.668 V for D_{it} of 1×10^{8} cm^{-2}/eV. This illustrated that if we only optimize poly-Si based passivating contacts, it is difficult to obtain the solar cells with superior V_{OC}. In Fig. 7(b), the impact of dopant concentrations of front p^+ emitter N_{p+} and densities of bulk defect state N_{tr} of Si substrate on V_{OC} was optimized. We can find the V_{OC} would increase to more than 0.720 V with the N_{tr} of 1×10^{8} cm^{-2}/eV and N_{p+} of 2×10^{21} cm^{-3} from the basis of ~0.670 V with N_{tr} of 1×10^{11} cm^{-2}/eV and N_{p+} of 2×10^{19} cm^{-3}, which proved that the front emitter and substrate quality also had an important influence on V_{OC}. The J_{SC} and *FF* can also be improved (omitted from the figure for clarity) by further optimizing the surface recombination rate *SRV*, SiO_x thicknesses *d* and Si substrate resistivity ρ, resulting in an improvement for the conversion efficiency η as shown in Fig. 7(c) and (d). The variation of rear *SRV* had little effect on the η, while the η increased from ~22% to over 24% for front *SRV* reducing from 1×10^5 cm/s to 10 cm/s, with significant effect. Different ρ values had little effect on η, but the substrate with low resistivity was better. Based on the above optimized parameters, the *J-V* and *P-V* curves of the *n*-PERT bifacial c-Si solar cells were finally calculated, as shown in Fig. 7(e) and (f). Front η can reach 24.64%, of which V_{OC} = 0.724 V, J_{SC} = 41.2 mA/cm^2, *FF* = 82.6%, and rear η = 22.33% with V_{OC} = 0.722 V, J_{SC} = 37.1 mA/cm^2, *FF* = 83.4%. The decline of rear efficiency mainly stemmed from the diminution of J_{SC}, which can be ascribed to the position of poly-Si based passivating contacts and the reduction in photon absorption from polished back surface compared to the textured front surface. However, the incident light both on front and back sides can bring a large amount of gain compared to monofacial solar cells. We have noticed that Trina solar recently reported the realization of large-area *n*-type crystalline Si industry-TOPCon (*i*-TOPCon) solar cells with cell efficiency reaching as high as 24.58% (Chen et al., 2019). This is in good agreement with our theoretical prediction.

4. Conclusions

In summary, we have successfully fabricated the large area (156×156 mm^2) *n*-PERT bifacial c-Si solar cells with top efficiency over 21% featuring front laser doping SE and back poly-Si based passivating contacts. The laser doping with appropriate energy can effectively reduce carrier recombination as well as improve interface passivation due to the lower resistivity Ohmic contact under the metal electrode area. The passivation quality of SiO_x/poly-Si stacks grown with nitric acid oxidation and PECVD technology, respectively, has been evaluated from the implied-V_{OC} and minority carrier lifetime τ_{eff} of solar cell precursors, together with the theoretical simulation to in-depth understand the nano-layer SiO_x passivation mechanism. The relatively higher implied-V_{OC} and τ_{eff} could be obtained via increasing the annealing temperature or annealing time of from 910 °C/20 min to 910 °C/30 min or from 890 °C/30 min to 910 °C/30 min. Solar cell would still maintain the high-efficiency for the SiO_x layer of 1.8 nm thick if the density of interfacial state D_{it} was decreased from 1×10^{10} cm^{-2}/eV to 1×10^{9} cm^{-2}/eV. We have finally calculated the *n*-type

bifacial solar cells with conversion efficiency of close to 25%, together with the yield of superior V_{OC} over 0.720 V, by means of optimizing not only rear poly-Si based passivating contacts, but also front emitter and Si substrate parameters. This demonstrated that the *n*-PERT bifacial c-Si solar cells with both SE and poly-Si based passivating contacts have a good development prospect for high-efficiency.

Acknowledgements

This work was supported by the Major State Basic Research Development Program of China (No. 2018YFB1500501) and Natural Science Foundation of China (11834011 and 11674225).

References

Adachi, D., Hernandez, J.L., Yamamoto, K., 2015. Impact of carrier recombination on fill factor for large area heterojunction crystalline silicon solar cell with 25.1% efficiency. Appl. Phys. Lett. 107 233506.

Blevin, T., Lanterne, A., Grange, B., Cabal, R., Vilcot, J.P., Veschetti, Y., 2014. Development of industrial processes for the fabrication of high efficiency n-type PERT cells. Sol. Energy Mater. Sol. Cells 131, 24–29.

Buchholz, F., Preis, P., Chu, H.F., Lossen, J., Wefringhaus, E., 2017. Progress in the development of industrial n-PERT cells. Energy Procedia 124, 649–656.

Chen, Y.F., et al., 2019. 24.58 % record efficiency for n-type i-TOPCon solar cells. ISFH. < http://chinaden.cn/news_nr.asp?id=22362&Small_Class=7 > .

Cuevas, A., 2014. Electrons and holes in solar cells with partial rear contacts. Prog. Photovoltaics: Res. Appl. 22, 764–774.

Du, C.H., Hsu, S.P., 2017. n-PERT solar cell using oxidation etch-back selective-BSF process. Energy Procedia 124, 406–411.

Edler, A., Mihailetchi, V.D., Koduvelikulathu, L.J., Comparotto, C., Kopecek, R., Harney, R., 2015. Metallization-induced recombination losses of bifacial silicon solar cells. Prog. Photovoltaics: Res. Appl. 23, 620–627.

Feldmann, F., Bivour, M., Reichel, C., Hermle, M., Glunz, S.W., 2014a. Passivated rear contacts for high-efficiency n-type Si solar cells providing high interface passivation quality and excellent transport characteristics. Sol. Energy Mater. Sol. Cells 120, 270–274.

Feldmann, F., Bivour, M., Reichel, C., Steinkemper, H., Hermle, M., Glunz, S.W., 2014b. Tunnel oxide passivated contacts as an alternative to partial rear contacts. Sol. Energy Mater. Sol. Cells 131, 46–50.

Feldmann, F., Bivour, M., Reichel, C., Hermle, M., Glunz, S.W., 2013. A passivated rear contact for high-efficiency n-type silicon solar cells enabling high VOCs and FF > 82%. 28th EU-PVSEC France: Paris.

Feldmann, F., Simon, M., Bivour, M., Reichel, C., Hermle, M., Glunz, S.W., 2014c. Efficient carrier-selective p- and n-contacts for Si solar cells. Sol. Energy Mater. Sol. Cells 131, 100–104.

Feldmann, F., Nogay, G., Loperc, P., Young, D.L., Lee, B.G., Stradins, P., Hermle, M., Glunz, S.W., 2018b. Charge carrier transport mechanisms of passivating contacts studied by temperature-dependent J-V measurements. Sol. Energy Mater. Sol. Cells 178, 15–19.

Feldmann, F., Nogay, G., Polzin, J.I., Steinhauser, B., Richter, A., Fell, A., Schmiga, C., Hermle, M., Glunz, S.W., 2018a. A study on the charge carrier transport of passivating contacts. IEEE J. Photovolt. 8, 1503–1509.

Fertig, F., Nold, S., Wohrle, N., Greulich, J., Haedrich, I., Krauss, K., Mittag, M., Biro, D., Rein, S., Preu, R., 2016. Economic feasibility of bifacial silicon solar cells. Prog. Photovoltaics: Res. Appl. 24, 800–817.

Fichtner, J., Zunft, H., Zuschlag, A., Knauss, H., Hahn, G., 2018. Gettering efficacy of APCVD-based process steps for low-cost PERT-type multicrystalline silicon solar cells. IEEE J. Photovolt. 8, 1464–1469.

Folchert, N., Rienacker, M., Yeo, A.A., Min, B., Peibst, R., Brendel, R., 2018. Temperature-dependent contact resistance of carrier selective poly-Si on oxide junctions. Sol. Energy Mater. Sol. Cells 185, 425–430.

Ghannam, M.Y., Shehadah, G., Abdulraheem, Y., Poortmans, J., 2013. Basic understanding of the role of the interfacial inversion layer in the operation of silicon solar cells with a-Si/c-Si heterojunction (HIT). In Proc. 28th EU-PVSEC France: Paris, 822–826.

Glunz, S.W., Rein, S., Lee, J.Y., Warta, W., 2001. Minority carrier lifetime degradation in boron-doped Czochralski silicon. J. Appl. Phys. 90, 2397–2404.

Haase, F., Hollemann, C., Schafer, S., Merkle, A., Rienacker, M., Krugener, J., Brendel, R., Peibst, R., 2018. Laser contact openings for local poly-Si-metal contacts enabling 26.1%-efficient POLO-IBC solar cells. Sol. Energy Mater. Sol. Cells 186, 184–193.

Hopman, S., Fell, A., Mayer, K., Fleischmann, C., Drew, K., Kray, D., Granek, F., 2009. Study on laser parameters for silicon solar cells with LCP selective emitters. In: Proc. 24th EU-PVSEC Germany: Hamburg, 1072–1076.

Huang, H.B., Modanese, C., Sun, S.H., von Gastrow, G., Wang, J.B., Pasanen, T.P., Li, S., Wang, L.C., Bao, Y.M., Zhu, Z., Sneck, S., Savin, H., 2018. Effective passivation of p^+ and n^+ emitters using $SiO_2/Al_2O_3/SiN_x$ stacks: Surface passivation mechanisms and application to industrial p-PERT bifacial Si solar cells. Sol. Energy Mater. Sol. Cells 186, 356–364.

Jaeger, U., Suwito, D., Benick, J., Janz, S., Preu, R., 2011. A laser based process for the formation of a local back surface field for n-type silicon solar cells. Thin Solid Films 519, 3827–3830.

Kiefer, F., Kruegener, J., Heinemeyer, F., Jestremski, M., Osten, H.J., Brendel, R., Peibst, R., 2016. Bifacial, fully screen-printed n-PERT solar cells with BF_2 and B implanted emitters. Sol. Energy Mater. Sol. Cells 157, 326–330.

Lanterne, A., Le Perchec, J., Gall, S., Coig, M., Tauzin, A., Veschetti, Y., 2014. 20.5% efficiency on large area n-type PERT cells by ion implantation. Energy Procedia 55, 437–443.

Lanterne, A., Le Perchec, J., Gall, S., Manuel, S., Coig, M., Tauzin, A., Veschetti, Y., 2015. Understanding of the annealing temperature impact on ion implanted bifacial n-type solar cells to reach 20.3% efficiency. Prog. Photovoltaics: Res. Appl. 23, 1458–1465.

Lerat, J.F., Desrues, T., Le Perchec, J., Coig, M., Milesi, F., Mazen, F., Michel, T., Roux, L., Veschetti, Y., Dubois, S., 2016. Boron emitter formation by plasma immersion ion implantation in n-type PERT silicon solar cells. Energy Procedia 92, 697–701.

Li, T., Wang, W.J., Zhou, C.L., Song, Y., Duan, Y., Li, Y.Z., 2013. Laser-doped solar cells exceeding 18% efficiency on large-area commercial-grade multicrystalline silicon substrates. Prog. Photovoltaics: Res. Appl. 21, 1337–1342.

Lozac'h, M., Nunomura, S., Sai, H., Matsubara, K., 2018. Passivation property of ultrathin SiOx:H/a-Si: H stack layers for solar cell applications. Sol. Energy Mater. Sol. Cells 185, 8–15.

Lu, G.L., Zheng, F., Wang, J.Q., Shen, W.Z., 2017. Thin Al_2O_3 passivated boron emitter of n-type bifacial c-Si solar cells with industrial process. Prog. Photovoltaics Res. Appl. 25, 280–290.

Moldovan, A., Feldmann, F., Krugel, G., Zimmer, M., Rentsch, J., Hermle, M., Roth-Folsch, A., Kaufmann, K., Hagendorf, C., 2014. Simple cleaning and conditioning of silicon surfaces with UV/ozone sources. Energy Procedia 55, 834–844.

Moldovan, A., Feldmann, F., Zimmer, M., Rentsch, J., Benick, J., Hermle, M., 2015. Tunnel oxide passivated carrier-selective contacts based on ultra-thin SiO_2 layers. Sol. Energy Mater. Sol. Cells 142, 123–127.

Peibst, R., Roemer, U., Larionova, Y., Schulte-Huxel, H., Ohrdes, T., Haeberle, M., Lim, B., Kruegener, J., Stichtenoth, D., Wuetherich, T., Schoellhorn, C., Graff, J., Brendel, R., 2014. Building blocks for back-junction back-contacted cells and modules with ion-implanted poly-Si junctions. In: Proc. IEEE 40th PVSC, pp. 852–856.

Reichel, C., Feldmann, F., Muller, R., Moldovan, A., Hermle, M., Glunz, S.W., 2015. Interdigitated back contact silicon solar cells with tunnel oxide passivated contacts formed by ion implantation. In: Proc. 29th EU-PVSEC, pp. 487–491.

Richter, A., Benick, J., Feldmann, F., Fell, A., Hermle, M., Glunz, S.W., 2017. n-type Si solar cells with passivating electron contact: identifying sources for efficiency limitations by wafer thickness and resistivity variation. Sol. Energy Mater. Sol. Cells 173, 96–105.

Richter, A., Benick, J., Mueller, R., Feldmann, F., Reichel, C., Hermle, M., Glunz, S.W., 2018. Tunnel oxide passivating electron contacts as full-area rear emitter of high-efficiency p-type silicon solar cells. Prog. Photovoltaics: Res. Appl. 26, 579–586.

Richter, S., Kaufmann, K., Naumann, V., Werner, M., Graff, A., Grosser, S., Moldovan, A., Zimmer, M., Rentsch, J., Bagdahn, J., Hagendorf, C., 2015. High-resolution structural investigation of passivated interfaces of silicon solar cells. Sol. Energy Mater. Sol. Cells 142, 128–133.

Rienacker, M., Bossmeyer, M., Merkle, A., Romer, U., Haase, F., Krugener, J., Brendel, R., Peibst, R., 2017. Junction resistivity of carrier-selective polysilicon on oxide junctions and its impact on solar cell performance. IEEE J. Photovolt. 7, 1–8.

Roemer, U., Peibst, R., Ohrdes, T., Lim, B., Kruegener, J., Bugiel, E., Wietler, T., Brendel, R., 2014. Recombination behavior and contact resistance of n^+ and p^+ poly-crystalline Si/mono- crystalline Si junctions. Sol. Energy Mater. Sol. Cells 131, 85–91.

Rudolph, D., Buck, T., Teppe, A., Masouleh, F.B., Harney, R., 2016. Firing through aluminum grid paste for bifacial solar cells. Energy Procedia 92, 971–977.

Schindler, F., Michl, B., Krenckel, P., Riepe, S., Feldmann, F., Benick, J., Warta, W., Schubert, M.C., 2015. Efficiency potential of p- and n-type high performance multicrystalline silicon. Energy Procedia 77, 633–638.

Schindler, F., Michl, B., Krenckel, P., Riepe, S., Benick, J., Muller, R., Richter, A., Glunz, S.W., Schubert, M.C., 2017. Optimized multicrystalline silicon for solar cells enabling conversion efficiencies of 22%. Sol. Energy Mater. Sol. Cells 171, 180–186.

Schindler, F., Fell, A., Muller, R., Benick, J., Richter, A., Feldmann, F., Krenckel, P., Riepe, S., Schubert, M.C., Glunz, S.W., 2018. Towards the efficiency limits of multicrystalline silicon solar cells. Sol. Energy Mater. Sol. Cells 185, 198–204.

Scht, J., Bothe, K., Bock, R., 2007. N-type silicon- the better material choice for industrial high-efficiency solar cells. 22th EU-PVSEC Italy: Milan.

Song, I., Lee, H., Lee, S.W., Bae, S., Hyun, J.Y., Kang, Y., Lee, H.S., Ohshita, Y., Ogura, A., Kim, D., 2018. Potential of chemical rounding for the performance enhancement of pyramid textured p-type emitters and bifacial n-PERT Si cells. Curr. Appl. Phys. 18, 1268–1274.

Stodolny, M.K., Lenes, M., Wu, Y., Janssen, G.J.M., Romijn, I.G., Luchies, J.R.M., Geerligs, L.J., 2016. n-type polysilicon passivating contact for industrial bifacial n-type solar cells. Sol. Energy Mater. Sol. Cells 158, 24–28.

Sugita, Y., Watanabe, S., Awaji, N., 1996. X-Ray reflectometry and infrared analysis of native oxides on Si (100) formed by chemical treatment. Jpn. J. Appl. Phys. 35, 5437–5443.

Tanaka, M., Taguchi, M., Matsuyama, T., Sawada, T., Tsuda, S., Nakano, S., Hanafusa, H., Kuwano, Y., 1992. Development of new a-Si/c-Si heterojunction solar cells: ACJ-HIT (artificially constructed junction-heterojunction with intrinsic thin-layer). Jpn. J. Appl. Phys. 31, 3518–3522.

Tong, J.N., Wang, X., Ouyang, Z., Lennon, A., 2015. Ultra-thin tunnel oxides formed by field-induced anodisation for carrier-selective contacts. Energy Procedia 77, 840–847.

Tous, L., Russell, R., Cornagliotti, E., Uruena, A., Choulat, P., Haslinger, M., John, J., Duerinckx, F., Szlufcik, J., 2017. 22.4% bifacial n-PERT cells with Ni/Ag co-plated contacts and Voc similar to 691 mV. Energy Procedia 124, 922–929.

Yoshikawa, K., Kawasaki, H., Yoshida, W., Irie, T., Konishi, K., Nakano, K., Uto, T., Adachi, D., Kanematsu, M., Uzu, H., Yamamoto, K., 2017. Silicon heterojunction solar cell with interdigitated back contacts for a photoconversion efficiency over 26%. Nat. Energy 2, 17032.

Young, D.L., Nemeth, W., LaSalvia, V., Reedy, R., Essig, S., Bateman, N., Stradins, P., 2016. Interdigitated back passivated contact (IBPC) solar cells formed by ion implantation. IEEE J. Photovolt. 6, 41–47.

Zhao, J.H., Wang, A.H., Altermatt, P.P., Green, M.A., Rakotoniaina, J.P., Breitenstein, O., 2002. High efficiency PERT cells on n-type silicon substrates. In: Proc. 29th IEEE PVSC New Orleans, pp. 218–221.